



Load transfer mechanism of geotextile-reinforced sand layer over semirigid column-improved soft soil

Pei-Chen Wu¹ · Wen-Bo Chen² · Wei-Qiang Feng³ · Jian-Hua Yin¹ · Tsz-On Ho⁴ · Shu-Ran Huang¹

Received: 4 December 2022 / Accepted: 25 December 2023 / Published online: 13 February 2024
© The Author(s), under exclusive licence to Springer-Verlag GmbH Germany, part of Springer Nature 2024

Abstract

Many design guidelines have been proposed for piled embankments, most of which consider piles or columns as rigid inclusions. In this study, a small-scale physical model test was performed to investigate the load transfer mechanism of a geotextile-reinforced sand layer over a soft subsoil improved by semirigid columns. A multi-stage load was applied at the top of the sand layer until the columns started to yield. When the columns yielded, a reverse load transfer was observed. Vertical stresses were measured and analyzed in terms of efficacy and stress reduction ratio (SRR) with a comparison of existing design guidelines for assessing soil arching. Among the reviewed guidelines, the approach recommended by the Dutch guidelines provided the closest results to the experimental data, whereas the one adopted by the American guidelines predicted well the change in efficacy and SRR under different surcharge loads. However, the load transfer mechanism after the yielding of columns is beyond the scope of the existing design guidelines. In addition, it was found through regression analysis that the increment of vertical stresses on columns and surrounding soil followed an inclined line under partially undrained conditions during loading stages and a curve during consolidation.

Keywords Geotextile · Load transfer mechanism · Physical model test · Soft soil · Semirigid columns

✉ Wen-Bo Chen
geocwb@gmail.com

Pei-Chen Wu
peichen.wu@connect.polyu.hk

Wei-Qiang Feng
fengwq@sustech.edu.cn

Jian-Hua Yin
cejhyin@polyu.edu.hk

Tsz-On Ho
tsz.on.ho@connect.polyu.hk; Ryan-TO.Ho@arup.com

Shu-Ran Huang
shu-ran.huang@polyu.edu.hk

- ¹ Department of Civil and Environmental Engineering, The Hong Kong Polytechnic University, Hong Kong, China
- ² College of Civil and Transportation Engineering, Shenzhen University, Shenzhen, China
- ³ Department of Ocean Science and Engineering, Southern University of Science and Technology, Shenzhen, China
- ⁴ Ove Arup & Partners Hong Kong Ltd (a Former Postdoctoral Fellow in Department of Civil and Environmental Engineering, The Hong Kong Polytechnic University), Hong Kong, China

1 Introduction

Recently, deep cement mixing (DCM) has been widely applied as a ground improvement technique in Hong Kong. In the third runway system project of Hong Kong International Airport, a layer of geosynthetic-reinforced (GR) load transfer platform (LTP) was designed over the soft soil treated using DCM columns before reclamation work [1, 47]. Similar to geosynthetic-reinforced column-supported (GRCS) embankments, the load transfer mechanism plays a significant role in reducing settlements, improving the bearing capacity of soft ground, and shortening the construction period.

The load transfer mechanism usually functions with the soil arching phenomenon in pile- or column-supported embankments with or without geosynthetic reinforcements [11, 26, 33, 39]. A family of friction models was established based on Terzaghi's soil arching theory [27, 29]. Then, the method of load–displacement compatibility (LDC) analysis was proposed by Filz et al. [8] to consider the relationship between settlement and soil arching in GRCS embankments. Another approach to investigate soil

arching is to conduct three-dimensional physical model tests. These tests take into account factors such as the consolidation of subsoils and the potential membrane effect of geosynthetic reinforcements (GRs). In these tests, subsoils are either real soils [59] or simulated using other materials, such as foams [24, 29, 34, 35] and water bags [42, 43]. In recent decades, full-scale and field tests have been conducted to explore the development of soil arching and the influence of cyclic loadings on the development of soil arching [42, 43, 60].

In the majority of experiments, piles are modeled by small concrete piles or rigid blocks. However, it is worth noting that the conclusions drawn from these experiments may not be directly applicable to semirigid or flexible columns, such as columns made of cement-treated soft soil, stones, or sand. Significant lateral deformations of stone columns and sand piles can have a substantial impact on the load transfer mechanism and the development of soil arching, particularly when the surrounding soil cannot provide sufficient confining pressure. The lateral deformations of semirigid columns, such as DCM columns, are relatively smaller than those of stone columns and sand piles. Many studies have focused on the bearing capacity and consolidation behavior of DCM column-treated soft soil under embankment loadings [12, 25, 48, 50, 55, 56]. Finite element methods were adopted to study the performance of GR embankments supported by DCM columns [22, 23, 41, 47, 50, 52]. However, the structuration and bonding formed within the cement-treated soil may break under significant loading levels, which can lead to failure or strain-softening behavior of cement-treated soils [16, 52]. Current design guidelines for GRCS embankments fail to capture the progressive failure and strain softening of DCM columns, which were reported and simulated by Yapage et al. [50, 51]. In addition, only a limited number of studies have focused on the load transfer mechanism in semirigid columns, geosynthetics, and soils.

In this study, a small-scale physical model test for a geotextile-reinforced (GR) sand layer over a soft subsoil improved using cement-treated soil columns was conducted to investigate the load transfer mechanism of semirigid column-supported embankments. A multi-stage surcharge load was applied until the columns yielded, which was identified by a sudden drop in vertical stress on the columns and a sudden increase in settlement.

2 Experiment setup and testing program

The physical model test was conducted in a steel tank with dimensions of 1000 mm (length) × 600 mm (width) × 800 mm (depth), as shown in Fig. 1. Six cement-treated soil columns were installed in the subsoil of Hong Kong

marine deposits (HKMD) overlaid by a GR sand layer. Similar setups were adopted by Zaeske [59] and van Eekelen et al. [34], in which the repeatability has been proved by dozens of tests. A multi-stage surcharge load was applied using a self-designed loading system equipped with a reaction frame and six pneumatic cylinders with a maximum output vertical stress of 200 kPa. The materials and transducers used in the model test are described in the following sections.

2.1 Materials

The subsoil in the physical model test was made through the reconstitution of the HKMD originally excavated from the coastal area of Lantau Island in Hong Kong [46]. HKMD is a type of dark gray soft soil with high compressibility and notable plasticity, whose basic properties are listed in Table 1. It should be noted that the effective cohesion of HKMD is nearly zero [6, 53]. The properties of the sand used in this study are listed in Table 1.

A piece of woven geotextile with a size of 1000 mm × 600 mm was prepared and framed with a pair of rectangular stainless-steel casing trims with an outer size of 950 mm × 550 mm and an inner size of 900 × 500 mm, as shown in Fig. 2. Considering the focus of this study is on the vertical deformation and the load transfer mechanism of vertical stresses acting on the columns, geotextile, and surrounding soils, it is imperative to control the movement of the geotextile in the horizontal direction in order to eliminate any potential impact on the strain within the geotextile and the load distribution. The casing trims were used to restrict the horizontal sliding/displacement of the geotextile but allow free vertical movement with the settlement of the underlying soil during the loading tests.

The tensile properties of the woven geotextile were determined using the wide-width strip method (ASTM D4595) [2]. The secant tensile modulus (J_s) of the geotextile is 680 kN/m in the longitudinal direction and 150 kN/m in the transversal direction. The tensile strength of the geotextile is 69 kN/m in the longitudinal direction and 17.3 kN/m in the transversal direction. Geotextiles with similar tensile moduli were used in small-scale physical model tests conducted by other researchers [24, 34, 35].

The semirigid columns adopted in this physical model were cement-treated soil columns with a diameter of 100 mm and a length of 400 mm. To ensure consistency of quality, the cement-treated soil columns with a cement content of 20% in terms of the dry mass of cement to the dry mass of HKMD were prefabricated individually, in a similar manner to cast concrete specimens. Reconstituted HKMD with an initial water content of 100% was thoroughly mixed with ordinary Portland cement (OPC) by a concrete mixer for 10 min. Cement–soil mixtures were

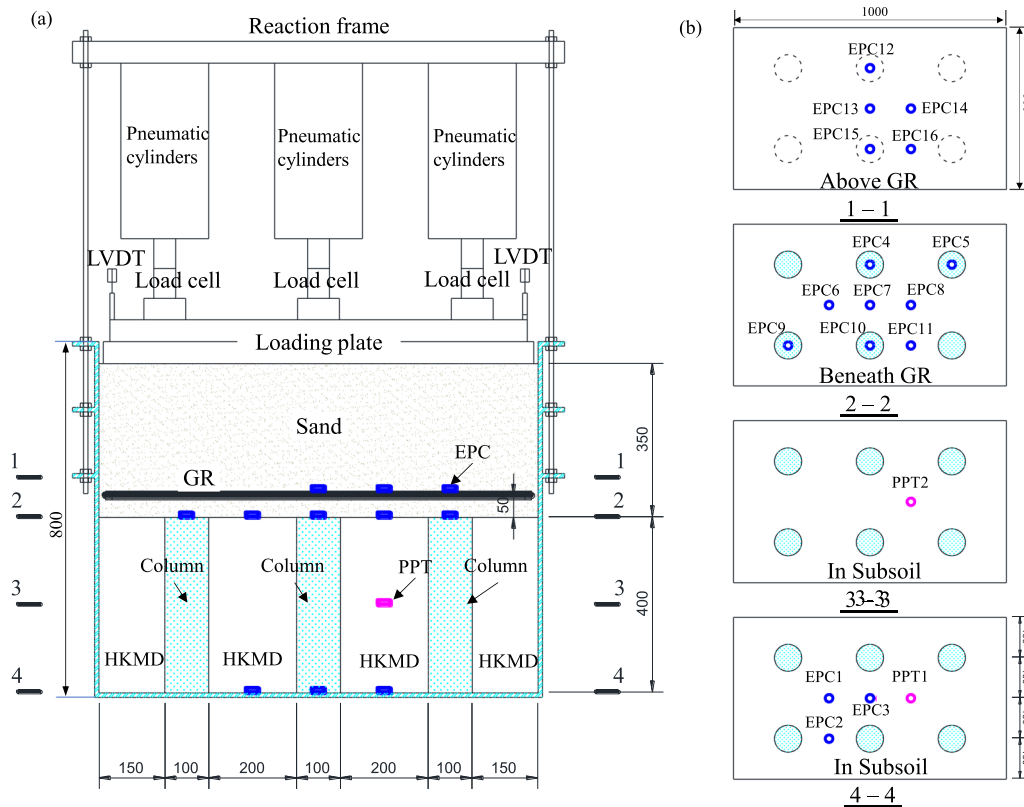


Fig. 1 Test setup and the layout of transducers (unit in mm)—a longitudinal cross section and b four horizontal cross sections

Table 1 Basic properties of Hong Kong marine deposits (HKMD) and sand

HKMD	G_s	Atterberg limits		PI (%)	w_0 (%)	pH	Loss of ignition (%)	φ' (°)	C_e/V	C_c/V	C_{ae}/V
		LL (%)	PL (%)								
	2.65	43.2	22.6	20.6	100	6.44	4.46	24	0.03	0.24	0.002
Sand	G_s	ρ_d (Mg/m ³)		w_{opt} (%)	d_{10} (mm)	d_{30} (mm)	d_{60} (mm)	φ' (°)			
		max	min								
	2.56	1.742	1.536	16.5	0.17	0.27	0.59	34.6			

G_s is the specific gravity, LL is the liquid limit, PL is the plastic limit, PI is the plasticity index, w_0 is the initial water content, C_e/V is the slope of unloading/reloading line, C_c/V is the slope of normal consolidation line of the reconstituted HKMD, C_{ae}/V is the creep coefficient, ρ_d is the dry density, and w_{opt} is the optimum water content.

subsequently cast into a PVC mold with an inner diameter of 100 mm by five layers. Immediately after filling each layer, the PVC mold containing the cement–soil mixtures was put on a vibration table and subjected to vibration for at least 60 s to avoid large voids in the mixture. The cement–soil mixture transformed into solid columns after 24 h. After being demolded from the PVC mold and wrapped with plastic sheet, the columns were stored in a chamber with a temperature of 20 °C and relative humidity of 90% for curing of 28 days. Similar approaches of fabricating cement-treated soil columns were adopted by Yin

and Fang [55] and Ho et al. [12], owing to the advantage of producing columns of uniform quality for physical model tests. The columns were installed in the physical model after 28 d of curing. Unconfined compression (UC) tests with a strain rate of 1 mm/min were conducted on cement-treated HKMD specimens with a diameter of 100 mm and a length of 200 mm after 28-day curing to obtain an average UC strength $q_u = 0.53$ MPa and a secant Young’s modulus $E_{50} = 70$ MPa. E_{50} was determined by the stress at 50% of the UC strength to the axial strain corresponding to this stress [13, 20, 31, 32].

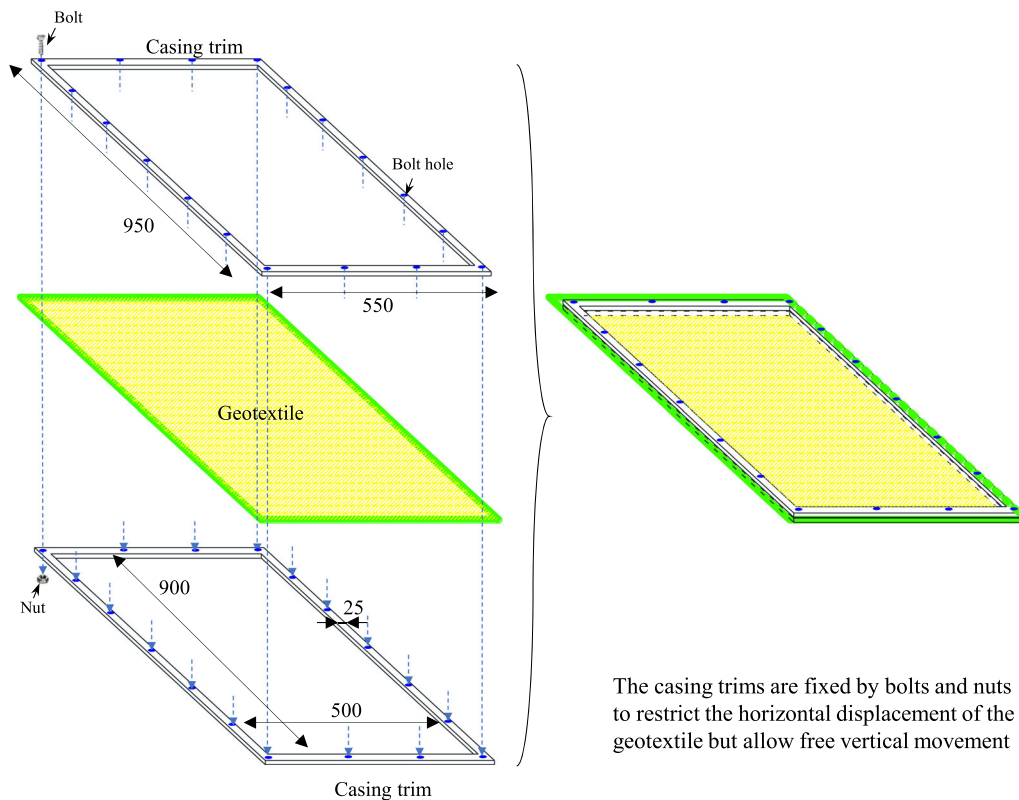


Fig. 2 Illustration of casing trims for fixing geotextile (unit in mm)

2.2 Transducers

Earth pressure cells (EPCs) with capacities of 0.2 MPa and 2 MPa were used to measure the vertical stresses at different locations. Two pore pressure transducers (PPTs) were placed at different locations in the subsoil. Linear variable differential transformers (LVDTs) were used to measure the settlements at the top surface of the sand layer. Load cells were used to record the loading output of the loading system. An NI PXIe 4331 datalogger was used to record the voltage signals from EPCs, PPTs, LVDTs, and load cells.

2.3 Model preparation and setup

Lubricant was applied to the side walls of the physical model tank to minimize the effect of the side friction between the walls and soils. Intact HKMD was thoroughly mixed with additional water to form a slurry with a water content of 100% and was subsequently carefully poured into the tank to minimize the air trapped inside the soil. The consolidation of the slurry under a uniform load of 5.35 kPa was then conducted. Prefabricated vertical drain bands (PVDs) were employed to speed up the consolidation process. PVDs were removed after consolidation. Metal pipes with an inner diameter of 100 mm were inserted

vertically into the subsoil guided by a wooden plate with circular holes. Level rulers were used to check the verticality of the pipes. Soil inside the metal pipes was extracted along with these pipes forming holes in the subsoil for the installation of prefabricated cement-treated soil columns. After carefully inserting the columns into the holes, cement slurry with a cement content of 20% was poured into the holes to fill the gap between the columns and the surrounding soil. It is worth mentioning that the method of installing cement-treated soil columns used in this study is different from the real practice of constructing DCM columns. The effect of in situ mixing procedures on the properties of the columns and surrounding soils is not considered in this study. Eight EPCs were placed at the top of the HKMD subsoil improved by cement-treated soil columns, as shown in Fig. 1.

To simulate the load transfer platform used in the third runway system project of Hong Kong International Airport, a sand blank with a thickness of 50 mm was placed on top of the subsoil before installing the geotextile and the EPCs for measuring the vertical stress over the geotextile. The total thickness of the sand layer reached 350 mm after filling another six layers of sand (each with a thickness of 50 mm). The construction of the sand layer took approximately 15 d. The total weight and volume of the sand were controlled to obtain a sand fill with a relative density of

80%, and a rigid porous plate was placed on the top of the sand to serve as a loading plate and a platform for setting the LVDTs.

2.4 Geometrics and scale effects

A certain height of embankments is required by the current design guidelines so that soil arching can be fully developed. The GR sand layer in this study was 0.35 m, which was higher than the minimum height recommended by BS 8006 [3], Dutch design guidelines [37], and the Federal Highway Administration (FHWA) of the United States [28] under the geometrical configuration of the physical model test, namely 0.15, 0.22, and 0.33 m, respectively.

Without scaling, stress and time in this physical model test were the same as those in the geotechnical prototype, which requires other variables to be scaled down accordingly [4, 45], as shown in Table 2. The same approach was also adopted by van Eekelen et al. [34] to avoid considering stress-dependent behavior of filling materials. They also clarified that it is not necessary to apply scaling rules when comparing the measured results with the results calculated by analytical models. The scale of the physical model test was approximately 1:6 for the diameter and spacing of the columns in an embankment reported by Jamsawang et al. [15].

3 Experiment results

3.1 Settlement and excess pore pressure

A multi-stage loading test was started five days after the construction of the sand layer using the self-designed loading system following a loading sequence of 10, 20, 40, and 80 kPa. Surface settlements were measured during the loading tests. Each loading test was conducted until the excess pore pressure was nearly fully dissipated. Figure 3a shows the actual load applied at the top of the sand layer

Table 2 Scaling of variables

Parameter	Scaling	Dimension
Time	1	[T]
Stress	1	[M/LT ⁻²]
Length	1:x	[L]
Stiffness of geotextile	1:x	[MT ⁻²]
Tensile strength of geotextile	1:x	[MT ⁻²]
Area	1:x ²	[L ²]
Force	1:x ²	[MLT ⁻²]
Strength of soil and columns	1	[M/LT ⁻²]

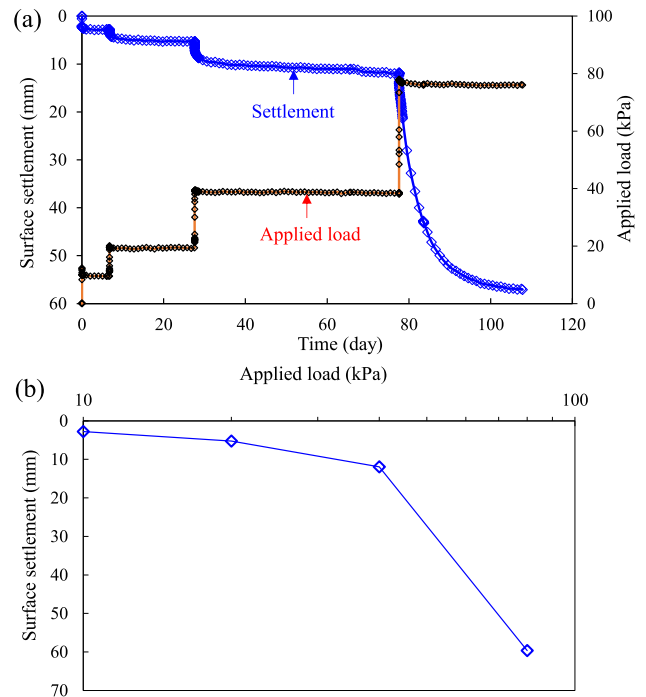


Fig. 3 a Measured surface settlement and applied load with time and b Surface settlement versus applied load (log scale)

and the surface settlement, measured using load cells and LVDTs, respectively. The surface settlement was below 20 mm under the applied load of 10, 20, and 40 kPa, showing the effectiveness of cement-treated soil columns in controlling settlement. A significant increase in surface settlement was observed when the applied load reached 80 kPa. Figure 3b plots the final settlement under each load stage. The shape of the settlement–log(load) curve is similar to typical *e*–log(σ) curves obtained from oedometer tests covering both over-consolidated and normally consolidated states. The composite ground of HKMD improved by cement-treated soil columns under the geotextile-reinforced sand fill exhibited a low compressibility

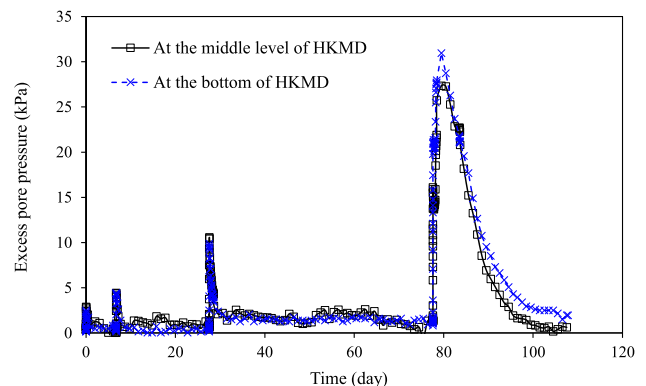


Fig. 4 Measured excess pore pressures with time at different locations in HKMD

when the applied load was lower than 40 kPa; however, it showed a high compressibility when the applied load reached 80 kPa. The significant difference could be attributed to the yielding of the cement-treated soil columns, which is discussed in the next section.

Figure 4 presents the excess pore pressures in the HKMD measured over time using PPT1 and PPT2. When the applied load was smaller than 80 kPa, no significant difference in the measured excess pore pressures was observed between the bottom level (PPT1) and middle level (PPT2) of the HKMD. Rapid dissipation of excess pore pressure at both levels was observed at the beginning of each loading stage. As the applied load approached 80 kPa, it was observed that the excess pore pressure measured at the bottom of the HKMD was greater than that measured at the middle level. In addition, the excess pore pressure at the middle level dissipated faster than that at the bottom. The observed responses of the excess pore pressure were probably attributed to the different drainage paths for the soils at different locations and yielding of the columns that changed the stress state and drainage situations for the PPTs at different locations. It should be noted that the yielded columns might have lateral expansion toward the

surrounding soil, resulting in an increase in lateral stress and pore water pressure inside the surrounding soil [6, 56].

3.2 Vertical stress

Vertical stresses measured using EPCs at different locations are presented in Fig. 5. Figure 5a, b shows the vertical stresses above the GR. There was no significant difference observed between the vertical stress measured by EPC12 and that measured by EPC15. A notable difference between the vertical stress measured by EPC13 and that measured by EPC14 was observed after 80 d when the cement-treated soil columns yielded. Figure 5c, d presents the vertical stresses (beneath the GR) at the top of the columns and the HKMD subsoil, respectively. Before the yielding of the columns, the vertical stress measured by EPCs on each column did not exhibit significant differences. However, when the columns started to yield, there was a non-negligible difference in the vertical stresses among different columns. This difference could be attributed to the eccentric loading after the yielding of the columns and different boundary effects. It should also be noted that the vertical stresses presented here were based

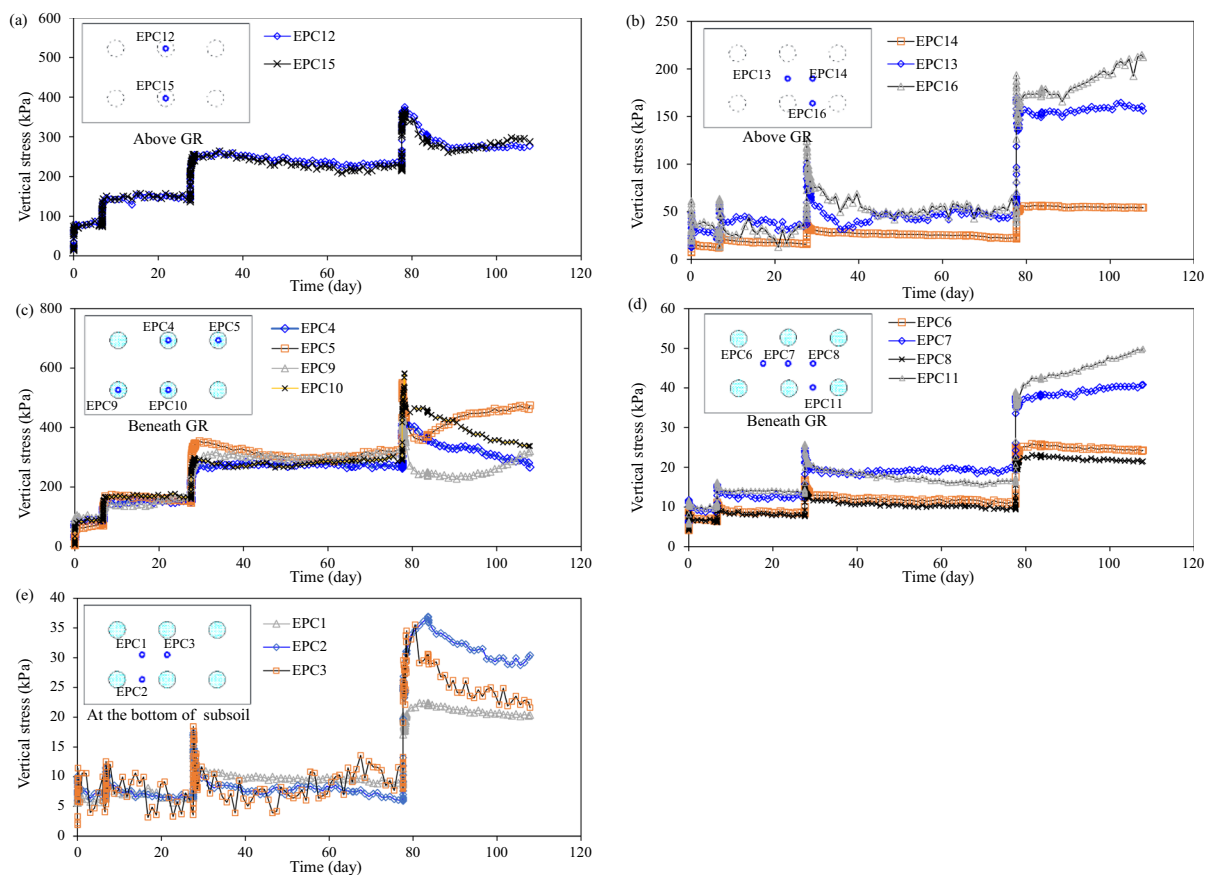


Fig. 5 Measured vertical stresses at the locations of **a** EPCs 12, 15; **b** EPCs 13, 14, and 16; **c** EPCs 4, 5, 9, and 10; **d** EPCs 6, 7, 8, and 11; and **e** EPCs 1–3

on local measurements. The limitations of the local measurements are discussed in Sect. 5. Figure 5e shows that the vertical stresses at the bottom of the HKMD subsoil were smaller than those at the top. This could be attributed to the skin friction between the columns and the surrounding soil. Comparing the excess pore pressure with the vertical total stress at the bottom of the HKMD subsoil, it can be observed that the excess pore pressure was higher than the vertical total stress at the beginning of the loading test. This could be attributed to additional lateral stress caused by the yielded columns and Mandel–Cryer effect [9] or creep effect of the HKMD [57].

To better address the mechanism of load transfer, the model test is divided into three zones: column, strip, and square zones, as shown in Fig. 6a. The column zone covers the cement-treated soil columns and the portion of the sand layer above the columns, the strip zone is the area between two adjacent column zones, and the square zone is the area enclosed by four strip zones. Strip and square zones are similar to those adopted by van Eekelen et al. [37]. It should be noted that the difference between vertical stresses above and beneath the geotextile in the column zone may be significant, depending on the development of the membrane effect of the geotextile. The circular cross section of columns can be converted into a square with an equivalent size of a . The area influenced by each column is illustrated using a column-soil unit, as shown in Fig. 6b.

Figure 7a shows the average vertical stress in the column zones. For the first two loadings, the vertical stresses above and beneath the geotextile show no discernible difference, indicating that the membrane effect of the geotextile was not fully mobilized. As the development of the membrane effect depends on the deflection of the geotextile related to the differential settlements between the

columns and surrounding soft soil, it can be deduced that the differential settlements during the first two loading stages were not remarkable. When the load increased to 40 kPa, a significant difference was observed between the vertical stresses above and beneath the geotextile, indicating that a certain settlement occurred, which induced a noticeable tension that caused the development of the membrane effect in the geotextile. Owing to the membrane effect, the load taken by the geotextile was transferred to adjacent columns, thereby increasing the vertical stress beneath the geotextile in the column zones. When the applied load was increased to 80 kPa, the vertical stresses above and beneath the geotextile in the column zones reached their peak values, indicating the yielding of columns. The yielding of columns induced a dramatic settlement on the surface of the sand layer, as shown in Fig. 3. After the test was completed, the column beneath EPC10 was retrieved from the physical model. This column had a typical shear failure, as shown in Fig. 7. After the test was completed, the column beneath EPC10 was retrieved from the physical model. This column had a typical shear failure, as shown in Fig. 7a. It is important to mention that the main focus of this study was on the load transfer before and after the yielding of cement-treated soil columns. The physical model test did not specifically delve into the failure modes of the soft ground improved by cement-treated soil columns, or the failure modes of each column installed in this test. Despite the yielding of the columns, the geotextile can continue to transfer the load to the columns. This load transfer could be due to the large differential settlements between the columns and surrounding soil as more loads could be transferred back to the surrounding soil. Considering the progressive failure of cement-treated soil columns, the membrane effect of the

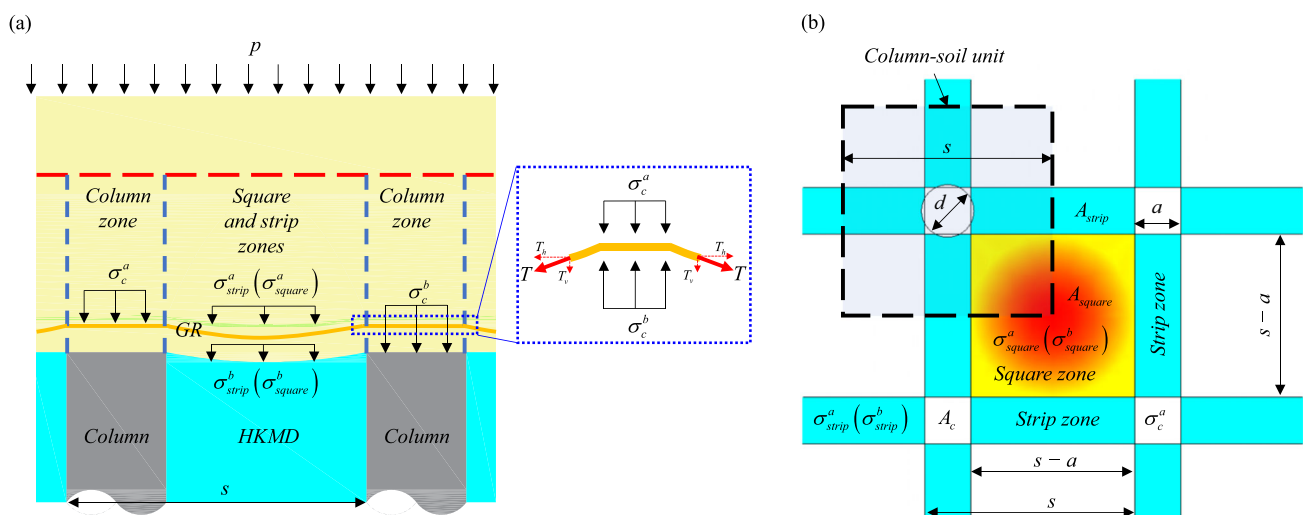


Fig. 6 Illustration of a column, square, and strip zones and b column-soil unit

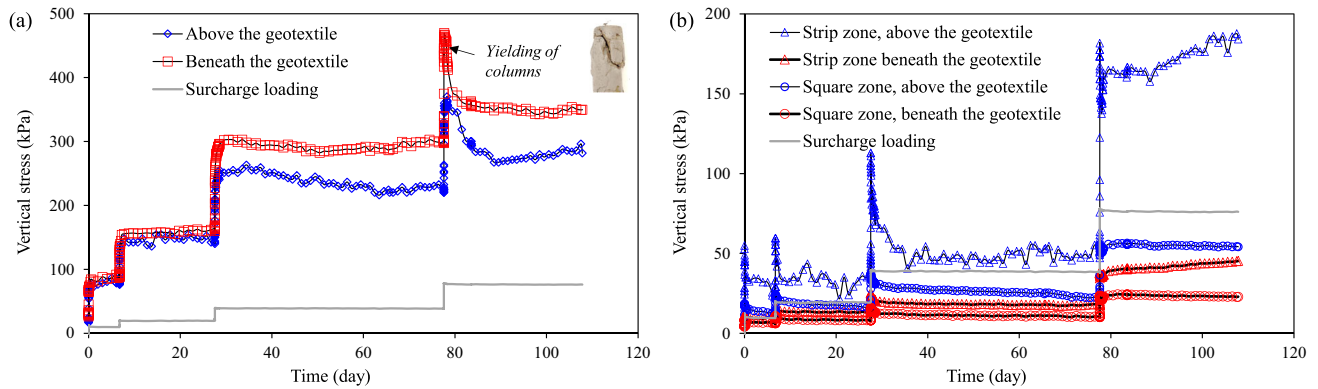


Fig. 7 Vertical stresses above and beneath the geotextile in **a** column zones and **b** strip and square zones

geotextile may accelerate the yielding of columns. In addition, the yielding stress of the columns in the physical model test was lower than the UC strength (0.53 MPa), which is uncommon as the strength of cement-treated soil columns under a confining pressure is normally higher than the unconfined compressive strength. Possible reasons could be: (1) The length-to-diameter ratio of the columns was 4:1, which was higher than that of the specimens for the UC tests (2:1), (2) the clamping effect inherent in UC tests, and (3) the local measurement of the vertical stress, which is discussed in Sect. 5.

Figure 7b shows the average vertical stresses above and beneath the geotextile in the strip and square zones, where the vertical stresses above the geotextile were greater than those beneath the geotextile. It is interesting to note that the vertical stress above the geotextile in the strip zone exceeded the applied load immediately after the load was applied. However, the increase in the vertical stress above the geotextile in the square zone did not exceed the applied surcharge load. At the beginning of each loading stage, the geotextile strips supported by two adjacent columns worked together with the columns, forming an “equivalent bridge” to participate in the transfer of load. In addition, given the partially undrained condition of the surrounding soil at that moment, the vertical stress above the geotextile in the strip zone was compatible with that above the geotextile in the column zone before the yielding of columns. However, as the excess pore water pressure dissipated, the soil in between the columns started to settle. This soil settlement initiated a load transfer process, wherein the load was transferred from the square zone of the geotextile to the strip zone and subsequently to the columns, resulting in a decrease in the vertical stresses above the geotextile in both the square and strip zones. As mentioned earlier, the yielding of the columns resulted in a reverse load transfer from columns to the geotextile when the surcharge load increased to 80 kPa. Thus, the reverse load transfer significantly increased the load above the geotextile in the

strip zone. However, the increase in vertical stress after the yielding of columns could also be attributed to the geometry change of the load distribution in the strip zones, which probably affected the local measurement of the vertical stress.

3.3 Load distribution

3.3.1 Load parts A, B, and C

According to van Eekelen [34, 35], the load transfer in embankments can be divided into load parts A, B, and C, which are the portions of the load acting on columns, transferred to GR, and supported by the subsoil, respectively, as illustrated in Fig. 8. In this study, the vertical stresses above and beneath the geotextile in the column zone were used to calculate load parts A and A + B, respectively, whereas those beneath the geotextile in the

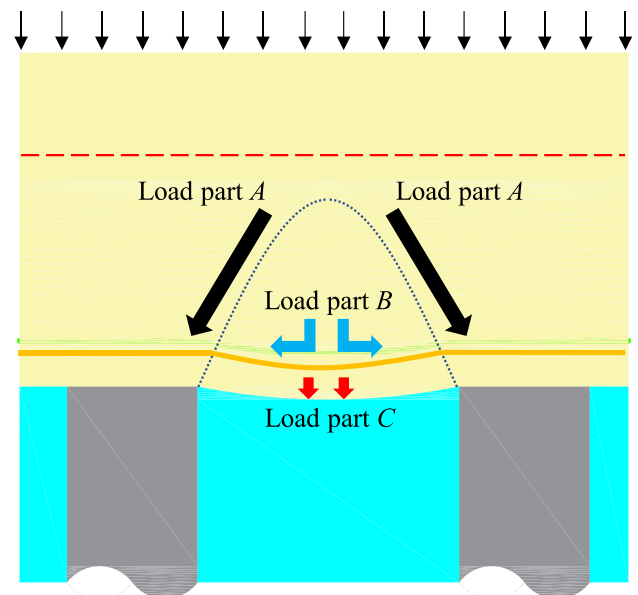


Fig. 8 Illustration of load parts A, B, and C

strip and square zones were used to determine load part C . The equations for determining load parts A , B , and C are provided as follows.

$$A = \sigma_c^a A_c \quad (1)$$

$$B = (\sigma_c^b - \sigma_c^a) A_c \quad (2)$$

$$C = \sigma_{\text{strip}}^b A_{\text{strip}} + \sigma_{\text{square}}^b A_{\text{square}} \quad (3)$$

where σ_c^a and σ_c^b are the vertical stresses above and beneath the geotextile in the column zone, respectively, σ_{strip}^b represents the vertical stress beneath the geotextile in the strip zone, σ_{square}^b is the vertical stress beneath the geotextile in the square zones, and A_c , A_{strip} , and A_{square} are the areas of the column, strip, and square zones within each column-soil unit, respectively. σ_{strip}^a and σ_{square}^a are the vertical stresses above the geotextile in the strip and square zones, respectively. σ_{strip}^a and σ_{square}^a are not included in the above equations but are used in the following discussion. σ_c^a , σ_c^b , σ_{strip}^b , σ_{square}^b , σ_{strip}^a , σ_{square}^a , A_c , A_{strip} , and A_{square} are illustrated in Fig. 6.

Figure 9 shows load parts A , B , and C (per column-soil unit) calculated using the vertical stresses measured at different locations and time points. In the first loading stage, there was no significant difference between load parts A and C , and load part B was nearly zero, indicating a slight effect of the geotextile. As the surcharge load increased, load part A became the largest portion among the three load parts. A significant reduction occurred in the load taken by the HKMD subsoil. The increase in load part B indicated that the geotextile started to contribute to the load redistribution. However, load part A decreased when the columns started to yield. After the yielding of columns, load part C became the dominant portion.

The sum of load parts $A + B + C$ and the total applied load per soil-column unit are shown in Fig. 9. When the applied load was 10 and 20 kPa, the sum of the load parts

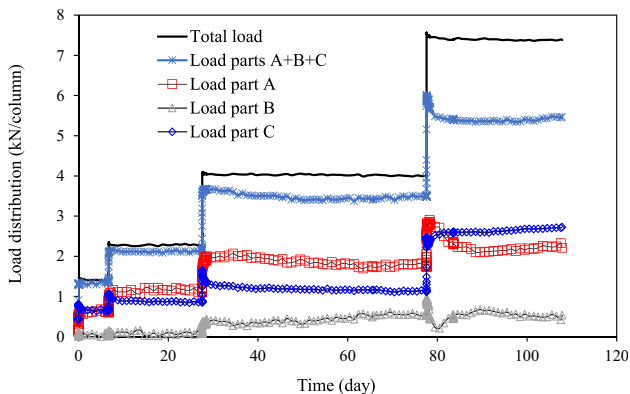


Fig. 9 Load distribution in a column-soil unit regarding load parts A , B , and C

$A + B + C$ agreed well with the applied load per soil-column unit. When the load was 40 kPa, the sum of the load parts $A + B + C$ was smaller than the applied load per soil-column unit. This was mainly due to the local measurement of the vertical stress using EPCs, which is discussed in Sect. 5. When the applied load reached 80 kPa, there was a significant difference between the sum of the load parts $A + B + C$ and the applied load per soil-column unit. This could be attributed to the yielding of the columns, which might change the area of the column zones.

3.3.2 Load transfer mechanism

To investigate the load transfer mechanism of the GR sand layer over the semirigid column-improved soft soil under surcharge loads, the vertical stresses in the column, strip, and square zones have been analyzed at different stages.

Figure 10a shows the relationships between the vertical stresses in the column and square zones (above the geotextile) in different stages. In each loading stage, the vertical stresses in both the column and square zones increased until the subsoil started to consolidate. The ratio of the increment of σ_c^a to the increment of σ_{square}^a was nearly identical in each loading stage. Linear regressions were conducted on σ_c^a and σ_{square}^a in the loading stages, as indicated by the dotted lines in Fig. 10a. The slope is similar to the stress concentration ratio, which is an important index representing the load distribution on the soft soil improved by columns [11, 54]. The average slope of the dotted lines in the four loading stages is 2.44. As the surcharge load increased in a short period of time, the subsoil was considered to be in a partially undrained condition during the loading stages. A linear envelope line with a slope of 6.16 can be drawn by fitting the relationship between σ_c^a and σ_{square}^a before consolidation at each loading stage (immediately after load application). Soil arching in the overlaid GR sand layer started to develop when the consolidation settlement of the subsoil increased, causing an unloading process to occur in the square zone. When the consolidation was completed, the load transfer paused, resulting in a stable state, which can be enveloped by a line with a slope of 13.73. In this physical model test, the slope of the envelope line after the consolidation of the subsoil was approximately doubled compared to that before consolidation. The two envelope lines before and after the consolidation of the subsoil formed a region where the vertical stress increments caused by the different surcharge loads followed a path of an inclined line under the partially undrained condition during loading stages and a curve during consolidation. However, the path crossed the lower boundary of the region (the envelope line describing the

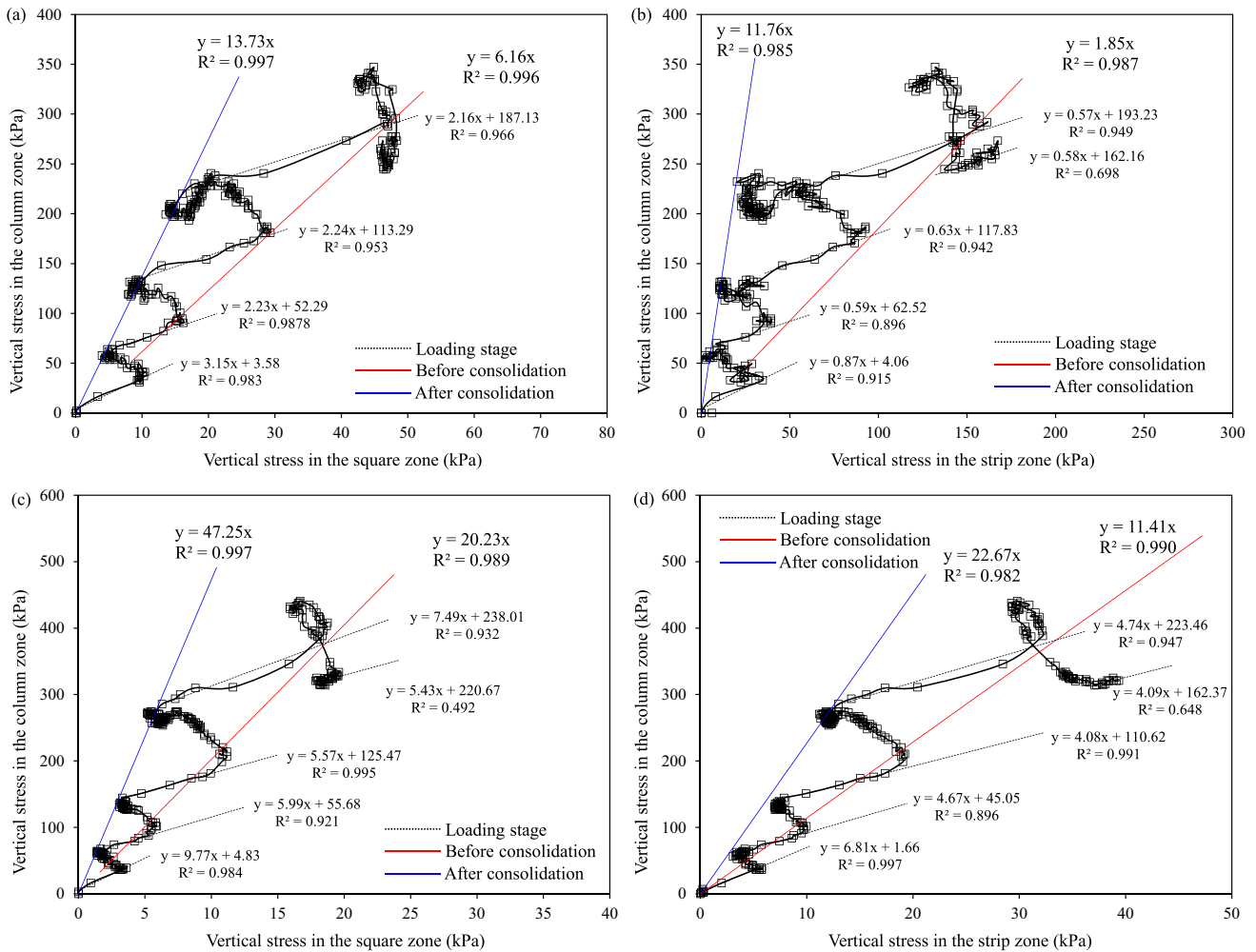


Fig. 10 Relationship between vertical stresses in **a** column zone versus square zone (above the geotextile), **b** column zone versus strip zone (above the geotextile), **c** column zone versus square zone (beneath the geotextile), and **d** column zone versus strip zone (beneath the geotextile)

state immediately after the application of load) as the columns started to yield.

Figure 10b shows the relationships between the vertical stresses in the column and strip zones (above the geotextile) at different stages. Linear functions can be used to fit the relationship between σ_c^a and σ_{strip}^a during the loading stages, as shown by the dotted lines in Fig. 10b. The dotted lines are nearly parallel with an average slope of 0.66, indicating that the vertical stress increment in the strip zone was larger than that in the column zone owing to the partially undrained condition during the loading stages. Two envelope lines with slopes of 1.85 and 11.76 representing the stages before and after the consolidation, respectively, are plotted. The slope of the envelope line after consolidation is approximately six times greater than that before consolidation, indicating that the consolidation of the subsoil largely affected the load transfer between the column and strip zones above the geotextile. An inclined line under the partially undrained condition during loading

stages followed by a curve during consolidation was also observed in the region formed by the two envelope lines before and after consolidation. After the columns yielded, the path shifted outside of the defined region.

Figure 10c shows the relationships between the vertical stresses in the column and square zones (beneath the geotextile) at different stages. Similarly, linear functions can be used to fit the relationship between σ_c^b and σ_{square}^b during the loading stages, as indicated by the dotted lines in Fig. 10c. These dotted lines are nearly parallel and have an average slope of 7.21, which represents the stress concentration ratio of the vertical stress in the column zone to that in the square zone. The value agrees with the typical stress concentration ratio of GRCS embankments with semirigid columns, which ranges from 5 to 10 [11]. Two envelope lines with slopes of 20.23 and 47.25 representing the stages before and after the consolidation, respectively, are plotted. The ratio between the slopes of the envelope lines before and after consolidation is approximately 2,

which is similar to the ratio obtained from Fig. 10a. In addition, a similar path of an inclined line under the partially undrained condition during the loading stages followed by a curve during consolidation can be also observed. The relationship between the vertical stresses in the column and square zones after the yielding of the columns is similar to that in the loading stages before yielding.

The relationships between the vertical stresses in the column and strip zones beneath the geotextile at different stages are fitted by dotted lines with an average slope of 5.07, as shown in Fig. 10d. Two envelope lines with slopes of 11.41 and 22.67, representing the stages before and after the consolidation, respectively, are plotted. The slope of the envelope line after consolidation is approximately 1.7 times greater than that before consolidation. A similar path of an inclined line under the partially undrained condition in the loading stages followed by a curve during consolidation can be also observed. The relationship between the vertical stresses in the column and square zones after the yielding of the columns is similar to those in the loading stages before yielding.

4 Assessment of arching effect

Many scholars have started to consider the strain-softening and progressive failure of column-supported embankments [51, 58, 61]. However, only the elastic behavior of columns/piles is considered in the current design methods for determining arching effect. Therefore, it is worth investigating the load transfer mechanism after the yielding of the columns with the comparison to the results provided by the current design methods in order to improve the design methods not only for guiding the design but also for analyzing and explaining the reasons behind failures and geohazards.

4.1 Assessment of arching effect using current design methods

According to Hewlett and Randolph method, pile (or column) efficacy E is the proportion of the load taken by columns. In this study, the efficacy of the cement-treated soil columns is calculated as follows:

$$E_A = \frac{A}{(\gamma H + p)s^2} \quad (4)$$

$$E_{A+B} = \frac{A+B}{(\gamma H + p)s^2} \quad (5)$$

where E_A is the efficacy in which the effect of geotextile is ignored, E_{A+B} is the efficacy in which the effect of

geotextile is considered, A and B represent load parts A and B determined by Eqs. (1) and (2), respectively, p is the surcharge load at the top of the GR sand layer, s is the size of the column-soil unit influenced by the column, γ is the unit weight of the embankment fill, and H is the height of the embankment.

SRR is an index used to assess the development of arching. $SRR = 1$ indicates that no arching effect occurs in the filling materials. A smaller SRR value indicates a more significant arching effect. In this study, SRR can be calculated as:

$$SRR = \frac{C}{(\gamma H + p)(s^2 - a^2)} \quad (6)$$

where C indicates load part C determined by Eq. (3).

Additionally, four commonly used methods from the current design guidelines for GRCS embankments are adopted to predict the efficacy E and stress reduction ratio SRR.

4.1.1 Hewlett and Randolph's method

A semi-spherical arching model was proposed to analyze the load transfer in GRCS embankments and adopted in the French guidelines and BS 8006 as an additional method. The critical location is assumed to be at the crown of semicircular arches or pile caps. Equations (4)–(9) are the equations for determining the efficacy and stress reduction ratio.

Critical location at the crown of arches:

$$E_{\text{crown}} = 1 - \left[1 - \left(\frac{a}{s} \right)^2 \right] (\alpha_1 - \alpha_1 \alpha_2 + \alpha_3) \quad (7)$$

$$SRR_{\text{crown}} = \alpha_1 - \alpha_1 \alpha_2 + \alpha_3 \quad (8)$$

$$\alpha_1 = \left[1 - \left(\frac{a}{s} \right)^2 \right]^{2(K_p - 1)}, \alpha_2 = \frac{s}{\sqrt{2}H} \left(\frac{2K_p - 2}{2K_p - 3} \right), \text{ and } \alpha_3 = \frac{s - a}{\sqrt{2}H} \left(\frac{2K_p - 2}{2K_p - 3} \right) \quad (9)$$

Critical location at pile caps:

$$E_{\text{cap}} = \frac{\beta}{1 + \beta} \quad (10)$$

$$SRR_{\text{cap}} = \frac{1}{(1 + \beta) \left[1 - (a/s)^2 \right]} \quad (11)$$

$$\beta = \frac{2K_p}{(K_p + 1)(1 + a/s)} \left[(1 - a/s)^{-K_p} - (1 + K_p a/s) \right] \quad (12)$$

where $K_p = \frac{1 + \sin(\phi')}{1 - \sin(\phi')}$, s is the column spacing, γ is the unit weight of the embankment fill, H is the height of the

embankment, a is the equivalent size of the column, and ϕ' is the friction angle of the embankment fill. The surcharge load is converted into an additional height $\Delta H = p/\gamma$ [42]. The efficacy and stress reduction ratio used for comparison are $\min(E_{\text{crown}}, E_{\text{cap}})$ and $\max(\text{SRR}_{\text{crown}}, \text{SRR}_{\text{cap}})$, respectively.

4.1.2 German EBGeo method

German EBGeo [5] adopted the multi-shell arches theory of Zaeske [59]. In EBGeo, subsoil support is considered only when calculating the tensile strain of GR. The efficacy and SRR are calculated as follows:

$$E = \frac{(\gamma H + p - \sigma_{z0})s^2 + \sigma_{z0}a^2}{(\gamma H + p)s^2} \quad (13)$$

$$\text{SRR} = \frac{\sigma_{z0}}{(\gamma H + p)} \quad (14)$$

$$\sigma_{z0} = \lambda_1^\lambda (\gamma + p/H) \left\{ H(\lambda_1 + h_g^2 \lambda_2)^{-\lambda} + h_g \left[(\lambda_1 + h_g^2 \lambda_2 / 4)^{-\lambda} - (\lambda_1 + h_g^2 \lambda_2)^{-\lambda} \right] \right\} \quad (15)$$

where $h_g = s_d/2$ for $H \geq s_d/2$, and $h_g = H$ for $H < s_d/2$, $\lambda = \frac{\alpha(K_{\text{crit}} - 1)}{\lambda_2 s_d}$, $K_{\text{crit}} = \tan^2(45^\circ + \frac{\phi'}{2})$, $\lambda_1 = \frac{(s_d - a)^2}{8}$, $\lambda_2 = \frac{s_d^2 + 2as_d - a^2}{2s_d^2}$, s_d is the center-to-center spacing between two diagonal columns, and p is the surcharge load.

4.1.3 Adapted Terzaghi method

Sloan et al. [30] extended Terzaghi's soil arching theory and proposed an adapted Terzaghi method, which has been adopted in FHWA design guidelines [28]. The pile efficacy determined by the adapted Terzaghi method can be expressed as follows:

$$E = 1 - \text{SRR} \left(1 - \frac{a^2}{s^2} \right) \quad (16)$$

$$\text{SRR} = \frac{\frac{\lambda}{\alpha} (1 - e^{-\alpha H}) + p e^{-\alpha H}}{(\gamma H + p)} \quad (17)$$

where $\alpha = p_c K_T \tan \phi' / (s^2 - a^2)$ and p_c is the column perimeter. $K_T = 0.75$ is suggested by Filz and Smith [7].

4.1.4 Concentric Arches (CA) model

The CA model is a three-dimensional (3D) soil arching model adopted in the Dutch design guidelines [37]. In the CA model, 3D concentric hemispherical arches are developed in square zones, whereas two-dimensional (2D) concentric semicircle arches are developed in strip zones. The pile efficacy is expressed as follows:

$$E = \frac{(\gamma H + p)s^2 - F_{\text{GRsquare}} - F_{\text{GRstrip}}}{(\gamma H + p)s^2} \quad (18)$$

and the stress reduction ratio is:

$$\text{SRR} = \frac{F_{\text{GRstrip}} + F_{\text{GRsquare}}}{(\gamma H + p)(s^2 - a^2)} \quad (19)$$

where F_{GRsquare} and F_{GRstrip} are the loads acting on the square and strip zones, respectively. van Eekelen et al. [36] presented in detail a method for determining F_{GRsquare} and F_{GRstrip} .

4.2 Pile efficacy

Figure 11a shows the changes in efficacy with surcharge load. When the surcharge was smaller than 40 kPa, the GR did not substantially increase the efficacy of the columns. As the surcharge increased, a significant difference between the efficacies with and without considering the membrane effect of the GR can be observed, indicating that the GR started to function. It was found that both the efficacies with and without considering the effect of the GR show a decrease during the process of increasing the surcharge load. This was due to the partially undrained condition of the subsoil, which delayed the load transfer. The differential settlements between the columns and surrounding soil increased with the consolidation of the subsoil, resulting in an increase in the deflection of the GR, and thus increasing the efficacy. The efficacy of the columns at the end of the consolidation slightly increased with an increase in surcharge load. This finding agreed with the results of a finite simulation conducted by van der Peet and van Eekelen [40]. A further increase in the surcharge load resulted in the yielding of the cement-treated soil columns.

Linear correlation relationships can be found between the efficacies with and without considering the membrane effect of the GR under different surcharge loads, as shown in Fig. 12. The ratios of the efficacies with and without considering the effect of GR are 1.16, 1.09, 1.19, and 1.28, under the surcharge loads of 10, 20, 40, and 80 kPa, respectively. The values generally agree with the range (1.15–1.3) reported by Low et al. [24] obtained from a series of 2D physical model tests. The development of the membrane effect of GR is related to its deflection and the differential settlement between the columns and surrounding soil. However, no direct measurement has been carried out on the deflection of GR, which is one of the limitations of this physical model test, as discussed in Sect. 5.

Among the four design guidelines, the result of the adapted Terzaghi method agreed well with the trend of the efficacy calculated using the measured data considering the GR effect (after consolidation) before the yielding of the

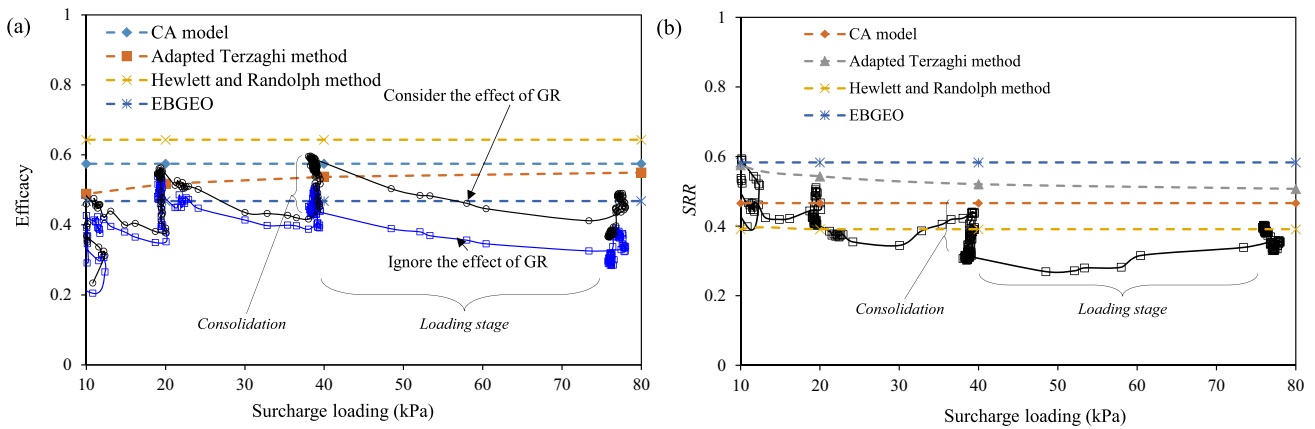


Fig. 11 a Efficacies and b stress reduction ratios calculated by measured data and estimated by different methods under different surcharge loads

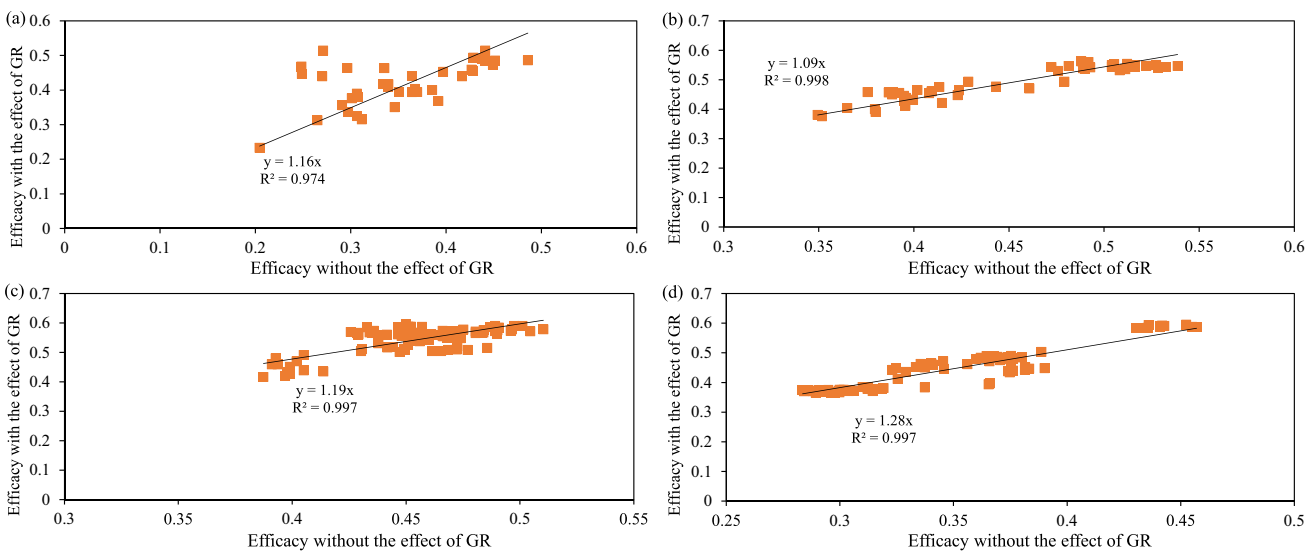


Fig. 12 Relationship between efficacies with and without the effect of GR under the surcharge loads of a 10 kPa, b 20 kPa, c 40 kPa, and d 80 kPa

cement-treated soil columns. However, it should be noted that the results calculated by the adapted Terzaghi method are highly dependent on the value of K_T . Higher K_T values result in higher efficacies. Therefore, this method must be used with caution. Despite its failure to capture the changing trend of efficacy considering the GR effect, the CA model gave results similar to those calculated using the measured data. The results of the German EBGEO [5] method agreed well with the efficacy calculated using the measured data disregarding the effect of the geotextile.

4.3 SRR

Figure 11b shows the SRR calculated using the measured data and the current design methods. The SRR calculated using the measured data tended to decrease with increasing surcharge load, indicating that more significant arching

occurred under a larger surcharge load. However, the SRR increased during the loading stages, which could be explained by the partially undrained condition within the short period of the loading stages. As the subsoil consolidated, the differential settlements between the columns and surrounding soil increased, resulting in an increase in the deflection of the geotextile, and thus reducing the SRR.

The adapted Terzaghi method captured the general decreasing trend of the SRR calculated using measured data. When the surcharge load was small (below 40 kPa in this study), both the CA model and Hewlett and Randolph’s method provided SRR values similar to those calculated using the measured data. However, the German EBGEO method gave an overestimated SRR compared with the other methods. van Eekelen et al. [4] reported similar results and explained that the German EBGEO

method does not take into account the increase in arching caused by consolidation.

4.4 Discussion

Hewlett and Randolph's method provided overestimated values in terms of the efficacy of semirigid columns. However, the vertical stress acting on the columns calculated by Hewlett and Randolph's method was generally smaller than those calculated by the German EBGEO [5] method and the CA model [40]. Thus, this method should provide lower efficacies. Under no surcharge load, Hewlett and Randolph's method resulted in an efficacy of 0.48, which was smaller than the efficacy calculated using the CA model. The overestimated results of Hewlett and Randolph's method were due to the height of the sand layer used in the calculation, which was increased by the additional height converted from the surcharge loads. Therefore, Hewlett and Randolph's method might not be suitable for embankments supported by semirigid columns subjected to large surcharge loads.

The efficacies and SRRs calculated by the CA model, German EBGEO method, and Hewlett and Randolph method remained constant under the different surcharge loads. This was because these methods are based on limit state equilibrium, which can only determine a constant arching stress value. The amount of deformation required to achieve the arching state assumed by these methods remains unclear [18]. The actual deformations that occur in GRCS embankments are incompatible with the required deformations, which leads to different results for various arching models. In addition, the decrease in efficacy and the increase in SRR due to the yielding of columns are beyond the scope of the current design guidelines.

In addition, it should be pointed out that the consistency or contradiction between the testing results and prediction by the design guidelines in this study should not be simply applied to other cases without performing additional investigations to take into account scale and boundary effects. However, the comparisons presented here may serve as a valuable reference for future endeavors, such as conducting full-scale experiments and numerical analysis on the load transfer mechanism of geotextile-reinforced sand layer over soft soil improved by semirigid columns.

5 Limitations of the physical model test

For small-scale physical model tests, one inevitable limitation is the scale effect. However, conducting small-scale tests is an economical way to address specific engineering issues and provide references for numerical modeling that bridges small-scale tests to real projects. Further

experimental and numerical studies should be conducted to investigate the influence of different factors, such as column configurations, material properties, and loading conditions on the load transfer mechanism. Two technical limitations are addressed in detail, as follows.

5.1 Local measurement of vertical stress

The distribution of vertical stress at the top of columns/piles is usually non-uniform. The vertical stress tends to be greater near the periphery of columns/piles [10]. As the size of the EPCs used in this study was smaller than the diameter of the cement-treated soil columns, the measured vertical stress only represented the local vertical stress at the center of each column instead of the overall average stress over each column. Therefore, the local measurement using small-sized EPCs probably underestimated the load taken by the cement-treated soil columns, indicating that the actual efficacies of the columns could be higher than those calculated using measured vertical stresses.

5.2 Deflection of GR

The development of soil arching in GRCS embankments is related to the deflection of the GR or the differential settlement between the columns and surrounding soil [14, 17]. Therefore, it is important to measure the deflection of GRs. However, no direct measurement was performed on the deflection of the GR in this small-scale physical model test. In full-scale experiments or field tests, settlement plates can be installed above the GR or in the subsoil to monitor the deflection of the GR or settlement of the subsoil. However, settlement plates were not applicable in this study with the current setup. Nevertheless, the maximum sag of the GR in the square zones can be estimated by the following equation proposed by King et al. [19]:

$$\delta_{s,\max} = 0.558 \sqrt[3]{\frac{\sigma_{\text{square}}^a (s-a)^4}{J}} \quad (20)$$

where $\delta_{s,\max}$ is the maximum sag of the GR in the square zones. The calculated maximum sags under the surcharge loads of 10, 20, 40, and 80 kPa are 2.79, 5.13, 7.87, and 18.08 mm, respectively. Comparing the maximum sags with the ratios of efficacies with and without considering the effect of GR, it can be roughly revealed that the membrane effect of the GR on efficacy increases with the deflection of the GR.

Although the tensile modulus of geotextiles/geogrids was reported to have little effect on the efficacy of columns [21, 34, 35], it could affect the soil arching by influencing the deflection of GR, as indicated by Eq. (20). Considering that the current design methods reviewed in Sect. 4 follow

the two-step design approach which assumes that arching actions are independent of the subsoil deformation and deflection of GR, the analysis on the load transfer mechanism in this study does not consider the influence of the tensile modulus of GR.

6 Findings and conclusions

A small-scale physical model test was conducted to investigate the load transfer mechanism of a GR sand layer over a soft subsoil improved by semirigid columns. A multi-stage surcharge load was applied to the sand layer until the yielding of columns was observed. The arching effect was assessed and compared with the current design methods for GRCS embankments. The main findings and conclusions are as follows:

- (a) Significant surface settlement was observed when the columns started to yield. The geotextile facilitated the load transfer between the columns and the subsoil.
- (b) When the columns yielded, the reverse load transfer from the column zone to the strip zone was significant.
- (c) Vertical stresses before and after the consolidation of the subsoil were enveloped with two lines, creating a region where the increments of the vertical stresses followed an inclined line under the partially undrained condition during loading stages, and a curve during consolidation.
- (d) Among the current design guidelines reviewed, the CA model of the Dutch guidelines provided efficacy and SRR that were closest to those obtained from the local measurement of vertical stress. The adapted Terzaghi method can predict well the change in efficacy and SRR under different surcharge loads. However, the decrease in efficacy and the increase in SRR due to the yielding of the columns are beyond the scope of the current design guidelines.

Acknowledgements The work in this paper is supported by a Research Impact Fund (RIF) project (R5037-18) and three General Research Fund (GRF) projects (PolyU 15210020; PolyU 15210322; PolyU 15226722) from Research Grants Council (RGC) of Hong Kong Special Administrative Region Government of China. The authors also acknowledge the financial support from Research Institute for Land and Space of The Hong Kong Polytechnic University and three grants (CD82, CD7A) from The Hong Kong Polytechnic University.

References

1. Airport Authority Hong Kong (2012) Expansion of Hong Kong international airport into a three-runway system project profile. <http://www.epd.gov.hk/eia/register/profile/latest/esb250/esb250.pdf>
2. ASTM (2005) 4595 Standard Test Method for Tensile Properties of Geotextiles by the Wide-Width Strip Method. ASTM Standards
3. BS 8006 (2010) Code of Practice for Strengthened/Reinforced Soils and Other Fills. British Standard Institution, UK
4. Butterfield R (1999) Dimensional analysis for geotechnical engineers. *Geotechnique* 49(3):357–366. <https://doi.org/10.1680/geot.1999.49.3.357>
5. EBGEO (2010) Empfehlungen für den Entwurf und die Berechnung von Erdkörpern mit Bewehrungen aus Geokunststoffen e EBGEO, vol. 2 German Geotechnical Society, Auflage 978-3-433-02950-3 (in German). Also available in English: Recommendations for Design and Analysis of Earth Structures using Geosynthetic Reinforcements e EBGEO, 2011. ISBN: 978-3-433-02983-1 and digital in English ISBN: 978-3-433-60093-1.
6. Feng WQ, Yin JH, Chen WB, Tan DY, Wu PC (2020) A new simplified method for calculating consolidation settlement of multi-layer soft soils with creep under multi-stage ramp loading. *Eng Geol* 264:105322. <https://doi.org/10.1016/j.enggeo.2019.105322>
7. Filz GM, Smith ME (2006) Design of bridging layers in geosynthetic-reinforced, column-supported embankments. Virginia Center for Transportation Innovation and Research. <http://hdl.handle.net/10919/46681>
8. Filz GM, Sloan JA, McGuire MP, Smith M, Collin J (2019) Settlement and vertical load transfer in column-supported embankments. *J Geotechn Geoenviron Eng* 145(10):04019083. [https://doi.org/10.1061/\(ASCE\)GT.1943-5606.0002130](https://doi.org/10.1061/(ASCE)GT.1943-5606.0002130)
9. Gibson RE, Gobert A, Schiffman RL (1989) On Cryer's problem with large displacements. *Int J Numer Anal Meth Geomech* 13(3):251–262. <https://doi.org/10.1002/nag.1610130303>
10. Han J, Gabr MA (2002) Numerical analysis of geosynthetic-reinforced and pile-supported earth platforms over soft soil. *J Geotechn Geoenviron Eng* 128(1):44–53. [https://doi.org/10.1061/\(ASCE\)1090-0241\(2002\)128:1\(44\)](https://doi.org/10.1061/(ASCE)1090-0241(2002)128:1(44))
11. Han J, Wayne MH (2000) Pile-soil-geosynthetic interactions in geosynthetic reinforced platform/piled embankments over soft soil. In Presentation at 79th annual transportation research board meeting, Washington, DC
12. Ho TO, Tsang DC, Chen WB, Yin JH (2020) Evaluating the environmental impact of contaminated sediment column stabilized by deep cement mixing. *Chemosphere* 261:127755. <https://doi.org/10.1016/j.chemosphere.2020.127755>
13. Ho TO, Chen WB, Yin JH, Wu PC, Tsang DC (2021) Stress-strain behaviour of cement-stabilized Hong Kong marine deposits. *Constr Build Mater* 274:122103. <https://doi.org/10.1016/j.conbuildmat.2020.122103>
14. Iglesia GR, Einstein HH, Whitman RV (2014) Investigation of soil arching with centrifuge tests. *J Geotechn Geoenviron Eng* 140(2):04013005. [https://doi.org/10.1061/\(ASCE\)GT.1943-5606.0000998](https://doi.org/10.1061/(ASCE)GT.1943-5606.0000998)
15. Jamsawang P, Yoobanpot N, Thanasisathit N, Voottipruex P, Jongpradit P (2016) Three-dimensional numerical analysis of a DCM column-supported highway embankment. *Comput Geotech* 72:42–56. <https://doi.org/10.1016/j.compgeo.2015.11.006>
16. Kamruzzaman AH, Chew SH, Lee FH (2009) Structuration and destructuration behavior of cement-treated Singapore marine clay. *J Geotechn Geoenviron Eng* 135(4):573–589. [https://doi.org/10.1061/\(ASCE\)1090-0241\(2009\)135:4\(573\)](https://doi.org/10.1061/(ASCE)1090-0241(2009)135:4(573))

17. King DJ, Bouazza A, Gniel JR, Rowe RK, Bui HH (2017) Load-transfer platform behaviour in embankments supported on semi-rigid columns: implications of the ground reaction curve. *Can Geotech J* 54(8):1158–1175. <https://doi.org/10.1139/cgj-2016-0406>
18. King DJ, Bouazza A, Gniel JR, Rowe RK, Bui HH (2017) Serviceability design for geosynthetic reinforced column supported embankments. *Geotext Geomembr* 45(4):261–279. <https://doi.org/10.1016/j.geotexmem.2017.02.006>
19. King L, King D, Bouazza A, Gniel J, Rowe RK (2021) Design of geosynthetic reinforced column supported embankments using an interaction diagram. *Geotext Geomembr* 49(1):159–165. <https://doi.org/10.1016/j.geotexmem.2020.09.010>
20. Kitazume M, Terashi M (2013) *The deep mixing method*. CRC Press, London
21. Lee T, van Eekelen SJM, Jung YH (2020) Numerical verification of the Concentric Arches model for geosynthetic-reinforced pile-supported embankments: applicability and limitations. *Can Geotechn J* 58(3):441–454. <https://doi.org/10.1139/cgj-2019-0625>
22. Liu KW, Rowe RK (2015) Numerical study of the effects of geosynthetic reinforcement viscosity on behaviour of embankments supported by deep-mixing-method columns. *Geotext Geomembr* 43(6):567–578. <https://doi.org/10.1016/j.geotexmem.2015.04.020>
23. Liu KW, Rowe RK, Su Q, Liu B, Yang Z (2017) Long-term reinforcement strains for column supported embankments with viscous reinforcement by FEM. *Geotext Geomembr* 45(4):307–319. <https://doi.org/10.1016/j.geotexmem.2017.04.003>
24. Low BK, Tang SK, Choa V (1994) Arching in piled embankments. *J Geotechn Eng* 120(11):1917–1938. [https://doi.org/10.1061/\(ASCE\)0733-9410\(1994\)120:11\(1917\)](https://doi.org/10.1061/(ASCE)0733-9410(1994)120:11(1917))
25. Phutthananon C, Jongpradist P, Jongpradist P, Dias D, Baroth J (2020) Parametric analysis and optimization of T-shaped and conventional deep cement mixing column-supported embankments. *Comput Geotech* 122:103555. <https://doi.org/10.1016/j.compgeo.2020.103555>
26. Rui R, Zhai YX, Han J, Van Eekelen SJM, Chen C (2020) Deformations in trapdoor tests and piled embankments. *Geosynth Int* 27(2):219–235. <https://doi.org/10.1680/jgein.19.00014>
27. Russell D, Pierpoint N (1997) An assessment of design methods for piled embankments. *Ground Eng* 30(10)
28. Schaefer VR, Berg RR, Collin JG, Christopher BR, DiMaggio JA, Filz GM, Bruce DA, Ayala D (2017) *Ground modification methods reference manual—Volume I and II*. Washington, DC: Federal Highway Administration. <https://www.fhwa.dot.gov/engineering/geotech/pubs/nhi16027.pdf>
29. Sloan JA (2011) *Column-supported embankments: full-scale tests and design recommendations*. Doctoral dissertation, Virginia Tech
30. Sloan J, Filz GM, Collin J (2011) A generalized formulation of the adapted terzaghi method of arching in column-supported embankments. In: *Geo-Frontiers 2011: Advances in Geotechnical Engineering*, pp 798–805 [https://doi.org/10.1061/41165\(397\)82](https://doi.org/10.1061/41165(397)82)
31. Sun Z, Chen WB, Zhao RD, Jin YF, Yin JH (2023) Solidification/stabilization treatment of Hong Kong marine deposits slurry at high water content by ISSA and GGBS. *Constr Build Mater* 372:130817. <https://doi.org/10.1016/j.conbuildmat.2023.130817>
32. Sun Z, Chen WB, Zhao RD, Shen P, Yin JH, Chen YG (2023) Effect of seawater on solidification/stabilisation treatment of marine soft soil slurry by lime-activated ISSA and GGBS. *Engineering Geology* 323:107216. <https://doi.org/10.1016/j.enggeo.2023.107216>
33. Terzaghi K (1943) Stress conditions for failure in soils. In: *Theoretical soil mechanics*. Wiley, New York, pp 11–15 <https://doi.org/10.1002/9780470172766.fmatter>
34. van Eekelen SJM, Bezuijen A, Lodder HJ, van Tol EA (2012) Model experiments on piled embankments. Part I. *Geotextiles Geomembranes* 32:69–81. <https://doi.org/10.1016/j.geotexmem.2011.11.002>
35. van Eekelen SJM, Bezuijen A, Lodder HJ, van Tol EA (2012) Model experiments on piled embankments. Part II. *Geotextiles Geomembr* 32:82–94. <https://doi.org/10.1016/j.geotexmem.2011.11.003>
36. van Eekelen SJM, Bezuijen A, Van Tol AF (2013) An analytical model for arching in piled embankments. *Geotext Geomembr* 39:78–102. <https://doi.org/10.1016/j.geotexmem.2013.07.005>
37. van Eekelen SJM, Bezuijen A, Van Tol AF (2015) Validation of analytical models for the design of basal reinforced piled embankments. *Geotext Geomembr* 43(1):56–81. <https://doi.org/10.1016/j.geotexmem.2014.10.002>
38. van Eekelen SJ, Brugman MH (2016) *Design guideline basal reinforced piled embankments*. CRC Press
39. van Eekelen SJ, Han J (2020) Geosynthetic-reinforced pile-supported embankments: state of the art. *Geosynth Int* 27(2):112–141. <https://doi.org/10.1680/jgein.20.00005>
40. van der Peet TC, van Eekelen SJM (2014) 3D numerical analysis of basal reinforced piled embankments. In: *Tenth international conference on geosynthetics*, pp 21–25
41. Waichita S, Jongpradist P, Schweiger HF (2020) Numerical and experimental investigation of failure of a DCM-wall considering softening behaviour. *Comput Geotech* 119:103380. <https://doi.org/10.1016/j.compgeo.2019.103380>
42. Wang HL, Chen RP, Liu QW, Kang X (2019) Investigation on geogrid reinforcement and pile efficacy in geosynthetic-reinforced pile-supported track-bed. *Geotext Geomembr* 47(6):755–766. <https://doi.org/10.1016/j.geotexmem.2019.103489>
43. Wang HL, Chen RP, Cheng W, Qi S, Cui YJ (2019) Full-scale model study on variations of soil stress in geosynthetic-reinforced pile-supported track bed with water level change and cyclic loading. *Can Geotech J* 56(1):60–68. <https://doi.org/10.1139/cgj-2017-0689>
44. Wijerathna M, Liyanapathirana DS, Jian Leo C (2017) Analytical solution for the consolidation behavior of deep cement mixed column-improved ground. *Int J Geomechan* 17(9):04017065. [https://doi.org/10.1061/\(ASCE\)GM.1943-5622.0000954](https://doi.org/10.1061/(ASCE)GM.1943-5622.0000954)
45. Wood DM (2003) *Geotechnical modelling*, vol 1. CRC Press
46. Wu PC, Yin JH, Feng WQ, Chen WB (2019) Experimental study on geosynthetic-reinforced sand fill over marine clay with or without deep cement mixed soil columns under different loadings. *Underground space* 4(4):340–347. <https://doi.org/10.1016/j.undsp.2019.03.001>
47. Wu PC, Feng WQ, Yin JH (2020) Numerical study of creep effects on settlements and load transfer mechanisms of soft soil improved by deep cement mixed soil columns under embankment load. *Geotext Geomembr* 48(3):331–348. <https://doi.org/10.1016/j.geotexmem.2019.12.005>
48. Wu PC, Feng WQ, Qin JQ, Liu KF, Yin JH (2023) A New Calculation Method for Life Cycle Settlement of Soft Ground with Creep Treated by Columns. *Int J Geomech*. <https://doi.org/10.1061/IJGNAL.GMENG-7899>
49. Yapage NNS, Liyanapathirana DS (2014) A parametric study of geosynthetic-reinforced column-supported embankments. *Geosynth Int* 21(3):213–232. <https://doi.org/10.1680/gein.14.00010>
50. Yapage NNS, Liyanapathirana DS, Kelly RB, Poulos HG, Leo CJ (2014) Numerical modeling of an embankment over soft ground improved with deep cement mixed columns: case history. *J Geotechn Geoenviron Eng* 140(11):04014062. [https://doi.org/10.1061/\(ASCE\)GT.1943-5606.0001165](https://doi.org/10.1061/(ASCE)GT.1943-5606.0001165)
51. Yapage NNS, Liyanapathirana DS, Poulos HG, Kelly RB, Leo CJ (2015) Numerical modeling of geotextile-reinforced

- embankments over deep cement mixed columns incorporating strain-softening behavior of columns. *Int J Geomechan* 15(2):04014047. [https://doi.org/10.1061/\(ASCE\)GM.1943-5622.0000341](https://doi.org/10.1061/(ASCE)GM.1943-5622.0000341)
52. Yapage NNS, Liyanapathirana DS (2019) A review of constitutive models for cement-treated clay. *Int J Geotech Eng* 13(6):525–537. <https://doi.org/10.1080/19386362.2017.1370878>
53. Yin JH (2001) Stress-strain-strength characteristics of soft Hong Kong marine deposits without or with cement treatment. *Lowland Technol Int* 3:1–13
54. Yin JH (2004) Properties and behavior of a cement mixed Hong Kong marine clay and design applications. In: *Proceedings of ground treatment*, Hong Kong Geotechnical Society, Hong Kong, pp 97–105.
55. Yin JH, Fang Z (2006) Physical modelling of consolidation behaviour of a composite foundation consisting of a cement-mixed soil column and untreated soft marine clay. *Geotechnique* 56(1):63–68. <https://doi.org/10.1680/geot.2006.56.1.63>
56. Yin JH, Fang Z (2010) Physical modeling of a footing on soft soil ground with deep cement mixed soil columns under vertical loading. *Mar Georesour Geotechnol* 28(2):173–188. <https://doi.org/10.1080/10641191003780872>
57. Yin JH, Graham J, Clark JI, Gao L (1994) Modelling unanticipated pore-water pressures in soft clays. *Can Geotech J* 31(5):773–778. <https://doi.org/10.1139/t94-088>
58. Yu X, Zheng G, Zhou H, Chai J (2021) Influence of geosynthetic reinforcement on the progressive failure of rigid columns under an embankment load. *Acta Geotech* 16(9):3005–3012. <https://doi.org/10.1007/s11440-021-01160-6>
59. Zaeske D (2001) Zur Wirkungsweise von unbewehrten und bewehrten mineralischen Tragschichten über pfahlartigen Gründungselementen. *Versuchsanst. Geotechnik, Univ. Gh Kassel, Fachgebiet u*
60. Zhang J, Zheng JJ, Chen BG, Yin JH (2013) Coupled mechanical and hydraulic modeling of a geosynthetic-reinforced and pile-supported embankment. *Comput Geotech* 52:28–37. <https://doi.org/10.1016/j.compgeo.2013.03.003>
61. Zheng G, Yang X, Zhou H, Chai J (2019) Numerical modeling of progressive failure of rigid piles under embankment load. *Can Geotech J* 56(1):23–34. <https://doi.org/10.1139/cgj-2017-0613>

Publisher's Note Springer Nature remains neutral with regard to jurisdictional claims in published maps and institutional affiliations.

Springer Nature or its licensor (e.g. a society or other partner) holds exclusive rights to this article under a publishing agreement with the author(s) or other rightsholder(s); author self-archiving of the accepted manuscript version of this article is solely governed by the terms of such publishing agreement and applicable law.